THE JOURNAL OF PHYSICAL CHEMISTRY C

Article

pubs.acs.org/JPCC

Discerning the Role of Ag−O−Al Entities on Ag/γ-Al_2O_3 Surface in NOx Selective Reduction by Ethanol

Hua Deng, Yunbo Yu, and Hong He*

State Key Joint Laboratory of Environment Simulation and Pollution Control, Research Center for Eco-Environmental Sciences, Chinese Academy of Sciences, Beijing 100085, China

Supporting Information

ABSTRACT: Alumina-supported silver catalysts (Ag/Al_2O_3) derived from AlOOH, $Al(OH)_3$, and Al_2O_3 were investigated for the selective catalytic reduction of NOx by ethanol. In order to discern the role of support Al skeleton in anchoring silver species and reducing NOx, the series of alumina-supported silver catalysts calcined at different temperatures was characterized by means of *in situ* DRIFTS, XPS, UV−vis DRS, XRD, BET, and NMR. It was found that the NO_x reduction efficiency order as affected by alumina precursors could be generally described as AlOOH > Al_2O_3 ≫ $Al(OH)_3$, with the optimum calcination temperature of 600 °C. XPS and UV−vis results indicated that silver ions predominated on the Ag/Al_2O_3 surface. Solid state NMR suggested that the silver ions might be anchored on Al tetrahedral and octahedral sites, forming Ag−O−Al_{tetra} and Ag−O−Al_{octa} entities. With the aid of NMR and DFT calculation, Al_{octa} was found to be the energetically favorable site to support silver ions. However, DFT calculation indicated that the Ag−O−Al_{tetra} entity can significantly adsorb and activate vital −NCO species rather than the Ag−O−Al_{octa} entity. A strongly positive correlation between the amount of Al_{tetra} structures and N_2 production rate confirms the crucial role of Al_{tetra} in NOx reduction by ethanol.

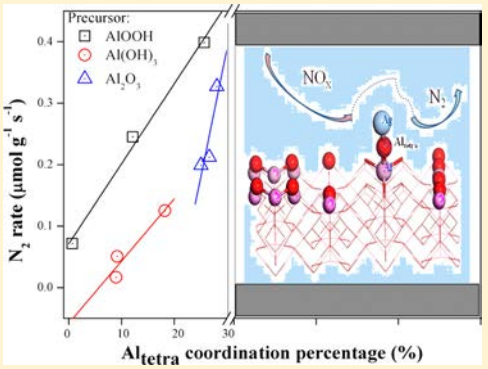

1. INTRODUCTION

When encountered with a potential energy crisis, the introduction of lean-burn gasoline engines and diesel engines becomes a popular strategy to improve fuel economy. Under an oxidizing atmosphere, however, NOx abatement is a major challenge for environmental catalysis.[1−5] Since the pioneering work of Iwamoto et al.[6] and Held et al.,[7] many catalysts such as zeolite-based catalysts,[6,8,9] supported precious metal catalysts, and metal oxides[1,3,10,11] have been developed for the SCR of NOx by hydrocarbons (HC-SCR). Among them, Ag/Al_2O_3 is deemed as one of the most effective materials for HC-SCR of NOx in excess oxygen.[12−15] As a result, many efforts have been made to draw a relationship between the structural features of Ag/Al_2O_3 catalysts and their catalytic activity in the SCR of NOx.

Serving as a support for silver, Al_2O_3 is better than other oxide supports like TiO_2, SiO_2, etc.[16,17] For HC-SCR over Ag/Al_2O_3, it has been accepted that silver (Ag) and Al on the support must interact strongly with each other to guarantee high activity for NOx reduction. Kinetic measurements performed by She and Flytzani-Stephanopoulos[18] confirmed that silver species, particularly Ag^+ cations, strongly bonded with the alumina support and possibly present as Ag−O−Al entities, are the active sites for SCR of NOx with methane. In surface mechanism studies, many important intermediates such as isocyanate species (−NCO) and enolic species (RCH═CH−O^-) have been identified, the formation of which was closely related to silver sites.[19,20] For instance, employing an elegant short time-on stream *in situ* spectroscopic transient isotope experimental technique, Burch et al.[19] confirmed that the interface between active silver and alumina contributes to the adsorption of reactive species like −NCO during H_2-assisted octane-SCR over Ag/Al_2O_3. Furthermore, using *in situ* DRIFTS and DFT calculation, Yan et al.[20] proposed that reactive enolic species prefer to adsorb on Ag sites or the interface between silver and the support. More recently, on the basis of theoretical simulation of the local structure of silver species and its interface with the support,[21] we found that the orbital mixing among Ag, O, and Al in Ag/Al_2O_3 is vital for the excellent catalytic performance of Ag/Al_2O_3. The results mentioned above suggest that the interaction of silver species with alumina is a key issue in revealing the intrinsic properties contributing to high efficiency HC-SCR over Ag/Al_2O_3. Nevertheless, the alumina support generally has different Al coordination environments such as octahedral (Al_{octa}) and/or tetrahedral (Al_{tetra}) Al coordination sites. Where the silver species locate and their corresponding activity are little reported indeed.

Calcination temperature is an important factor that affects the Al coordination environment. Transition aluminas (Al_2O_3)

Received: November 15, 2014
Revised: January 9, 2015
Published: January 14, 2015

DOI: 10.1021/jp5114416
J. Phys. Chem. C 2015, 119, 3132−3142

with high surface area, namely γ-, δ-, and η-Al_2O_3, are generated by thermal treatment of alumina precursors (commonly aluminum hydroxides) below 800 °C, during which the Al coordination environment partly changes from Al_{octa} to Al_{tetra}. The corresponding catalytic performance has been little correlated with the Al coordination. Even though calcination temperature has been proved to affect the activity of Ag/Al_2O_3 catalysts profoundly for NOx reduction.[22] Moreover, Zhang and Kaliguine[23] also have observed that silver catalysts derived from AlOOH and calcined at 500 °C exhibited the best SCR activity by propene due to high density of Ag−O−Al. Using *in situ* FTIR spectroscopy, Bion et al.[24] have studied the formation of the isocyanate species on Ag/Al_2O_3 catalysts using ethanol as reducing agent. It was proposed that −NCO species prefer to form on Al^{3+}_{tetra} sites. In addition, Iglesias-Juez et al.[25] have investigated NOx reduction by propene over Ag/Al_2O_3 catalysts using X-ray absorption spectroscopy under reaction conditions. Silver aluminate-like phases with tetrahedral structure (Al_{tetra}) are thought to be the active silver phase. On the basis of these important results, we can deduce that the high density of Ag−O−Al species probably Ag−O−Al_{tetra} entities on Ag/Al_2O_3 catalyst are supposed to be crucial for NO reduction to N_2. However, up to now, the detailed relationship between Ag−O−Al structure and the corresponding activity, including vital intermediate formation and N_2 production, has not been well understood.

In this study, the metal−support interaction was addressed based on a series of catalysts derived from different precursors and calcination temperatures. It was found that an Al_{penta}-coordination site is clearly the anchoring site to bond silver ions and form the Ag−O−Al_{oct} entity. Moreover, Al_{tetra} structures are directly linked with N_2 production.

2. MATERIALS AND METHODS

2.1. Materials Preparation. Ag/Al_2O_3 catalysts with constant loadings (2 wt % loading) were prepared by an impregnation method.[26,27] Pure AlOOH (SASOL, SB-1), $Al(OH)_3$ (Sigma-Aldrich), and γ-Al_2O_3 (SASOL, SBa-200) were used as precursors of Al_2O_3, an appropriate amount of which was immersed into an aqueous solution of silver nitrate. After stirring for 1 h, the excess water was removed by a rotary evaporator under vacuum at 60 °C. Then the samples were calcined in a furnace at 300, 400, 600, or 900 °C for 3 h, respectively. The final samples were denoted in the form of alumina precursor temperature. For example, the sample denoted as AlOOH-300 means AlOOH used as a precursor of Al_2O_3 and calcined at 300 °C after silver was loaded. For the convenience of comparison, the corresponding pure alumina samples derived from the precursors AlOOH, $Al(OH)_3$, and γ-Al_2O_3 were also prepared by the same procedure. Before activity tests, the catalysts were ground and sieved to a diameter range from 0.25 to 0.42 mm.

2.2. Catalytic Measurements. A gaseous mixture of NO (800 ppm), C_2H_5OH (1565 ppm), water vapor (10%), and O_2 (10%) in N_2 balance at a mass flow of 1 L min^{-1} was fed as described in our earlier studies.[20,28] The catalytic activity was measured in a fixed-bed reactor, where Ag/Al_2O_3 catalyst with weight of 0.3 g was packed in the bed (GHSV = 100 000 h^{-1}). The concentrations of NO, NO_2, N_2O, NH_3, and CO were analyzed online simultaneously by an FTIR spectrometer (Nicolet Nexus is10). The details of the experiment setup can be found in our earlier work.[20,28] In all the experiments, the concentration of N_2O was negligible; thus, NO_x conversion can be calculated using the equation

$$\text{NOx conversion (\%)} = \frac{[NO]_{in} + [NO_2]_{in} - [NO]_{out} - [NO_2]_{out}}{[NO]_{in} + [NO_2]_{in}} \times 100\%$$

The N_2 selectivity is defined as follows:

$$N_2\ \text{selectivity (\%)} = \frac{[NO]_{in} + [NO_2]_{in} - [NO]_{out} - [NO_2]_{out} - [NH_3]_{out}}{[NO]_{in} + [NO_2]_{in}} \times 100\%$$

Nitrogen production rate was calculated from the product analyses using the differential reactor approximation as follows:[29,30]

$$\text{rate (mol g}^{-1}\ \text{s}^{-1}) = \frac{F_T y}{W}$$

where F_T is the total molar flow rate (mol/s), y is the mole fraction of component N_2, and W is the weight of the catalyst (g). It is worthy of note that the NOx conversion over all catalysts were kept below 15% to eliminate the influence of mass and thermal transfer, and the experimental conditions can be found in our previous study.[20]

2.3. Catalyst Characterization. The X-ray powder diffraction patterns of the various catalysts were collected on a Rigaku D/max-RB X-ray diffractometer (Japan). The patterns were run with Cu Kα radiation (λ = 1.5406 Å) at 40 kV and 40 mA with a scanning speed of 5°/min. The patterns were taken over the 2θ range from 10° to 90°.

Nitrogen adsorption−desorption isotherms were measured using a Quantachrome Autosorb-1C instrument at 77 K. The specific surface area of the samples was calculated by the Brunauer−Emmett−Teller (BET) method. The volume of pores was determined by the Barrett−Joyner−Halenda (BJH) method from the desorption branches of the isotherms.

In situ DRIFTS spectra were recorded on a Nexus 670 FT-IR (Thermo Nicolet), equipped with an *in situ* diffuse reflection chamber and a high-sensitivity MCT/A detector. All Ag/Al_2O_3 catalysts were finely ground and placed in ceramic crucibles in the *in situ* chamber. Prior to recording each DRIFTS spectrum, the sample was heated *in situ* in 10% O_2/N_2 flow at 823 K for 1 h and then cooled to the desired temperature to measure a reference spectrum. All spectra were measured with a resolution of 4 cm^{-1} and with an accumulation of 100 scans.

XPS analyses were performed by means of an X-ray source using Al Kα radiation with energy of 1486.6 eV and power of 200 W. The continuum spectrum was fitted according to the Gaussian−Lorentzian files.

UV−vis diffuse reflectance spectra were measured by a U-3100 UV−vis spectrophotometer (Hitachi, Japan) with $BaSO_4$ as reference at room temperature in air. All spectra were collected in the range of 190−800 nm with a resolution of 1 nm. Because the γ-Al_2O_3 support exhibited strong absorbance below 300 nm that overlapped with that of the silver species, in order to understand the UV−vis results clearly, the spectrum of pure alumina was subtracted from the spectra of Ag/γ-Al_2O_3 samples. Prior to recording each UV−vis spectrum, the sample was finely grounded and heated in furnace at the corresponding calcination temperature for 1 h.

All ^{27}Al MAS NMR experiments were performed at room temperature on a Bruker 400 MHz WB solid-state NMR spectrometer, operating at a magnetic field of 9.4 T. The

DOI: 10.1021/jp5114416
J. Phys. Chem. C 2015, 119, 3132−3142

corresponding ^{27}Al Larmor frequency was 104.29 MHz. All of the spectra were acquired at a sample spinning rate of 10 kHz. A single pulse sequence with a pulse width of about 15° was used. Each spectrum was acquired using a total of 2000 scans with a recycle delay time of 0.5 s and an acquisition time of 0.018 s. All spectra were externally referenced (i.e., the 0 ppm position) to an 1 M $Al(NO)_3$ aqueous solution. The raw spectral data were normalized by weight since the weight of each sample was recorded.

DFT calculations were performed using Materials Studio (MS) Modeling CASTEP from Accelrys. Periodic boundary conditions in the generalized gradient approximation (GGA) were applied using the Perdew−Wang (PW91) function in our cases. All initial parameters had been checked by convergence tests. The electron−ion interaction was described by the ultrasoft potential in reciprocal space. A tight convergence of the plane-wave expansion was obtained with a kinetics energy cutoff of 400 eV. The dehydrated (110) and (100) surfaces of γ-alumina were established according to previously proven models.[31,32] Eight-layer-thick slabs (formula $Al_{32}O_{48}$) were constructed in this study. The interslab distance was maintained at 15 Å to avoid interslab interactions in the periodic systems. On the basis of the convergence test for k-point sampling, the k-point sets of (2 × 2 × 1) and (4 × 2 × 2) were used for the Al_2O_3 (110) and (100) surfaces (1 × 1), respectively. The adsorbate Ag ion was modeled both in the isolated state and supported on both Al_2O_3 surfaces, on which isolated Ag ion was optimized in a 20 × 20 × 20 Å cubic cell. The Brillouin-zone k-point mesh sampling was restricted to the gamma point. In order to compare the structure stability, the adsorption energy of Ag ions on the γ-Al_2O_3 support was calculated as follows:

$$E_{ad} = E_{adsorbate+surface} - (E_{surface} + E_{adsorbate})$$

The negative E_{ad} values indicate that the adsorbed state is energetically favorable. −NCO adsorbed on Ag/Al_2O_3 catalysts were performed using the supercell (2 × 2); the parameters were consistent with former results as mentioned above.

3. RESULTS AND DISCUSSION

3.1. Catalytic Activity of Ag/Al_2O_3. To investigate the metal (silver) and support (Al_2O_3) interaction (MSI), different kinds of alumina precursors, including AlOOH, $Al(OH)_3$ and Al_2O_3, were selected to examine the effect of the support. Furthermore, effects of calcination temperature on catalysts were also used to aid the investigation. Figures S1A−C display the conversion of NOx over Ag/Al_2O_3 prepared in different conditions, as a function of temperature in the ethanol-SCR process (N_2 selectivity as shown in Figure S2). Over all Ag/Al_2O_3 catalysts, increasing the calcination temperature from 300 to 600 °C significantly enhanced the NOx conversion. However, further increasing the calcination temperature to 900 °C decreased the NOx conversion over the whole temperature range. Among all precursors, the most significant promotion of NOx conversion was observed over samples derived from AlOOH. For instance, the NO_x conversion at temperature of 300 °C for AlOOH-300, $Al(OH)_3$-300, and Al_2O_3-300 was 11%, 10%, and 40%, respectively. When the calcination temperature for catalysts was increased to 600 °C, the corresponding NOx conversion rose to 97%, 54%, and 94%, respectively. Therefore, the order of NOx conversion efficiency related to alumina precursors at the optimum calcination temperature of 600 °C can be generally described as follows: AlOOH > Al_2O_3 ≫ $Al(OH)_3$. To further evaluate the catalytic performance among different catalysts, the rates of N_2 production at the reaction temperature of 300 °C (not higher than the lowest calcination temperature) are shown in Figure 1.

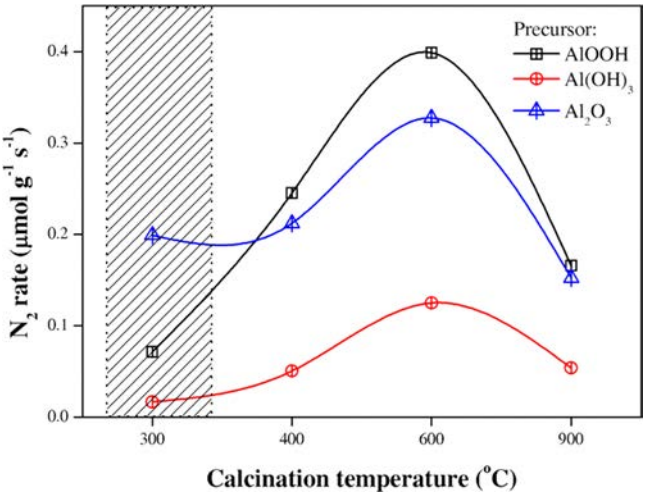

Figure 1. N_2 production rate at 300 °C over 2 wt % Ag/Al_2O_3 catalysts calcined at different temperatures. Conditions: NO 800 ppm, C_2H_5OH 1565 ppm, O_2 10%, H_2O 10%, N_2 balance.

As we clearly see, strongly peaked behavior (the N_2 production rate vs calcination temperature) was observed for all Ag/Al_2O_3 catalysts, with a maximum at 600 °C. The N_2 production rate order among different catalysts can be listed generally as AlOOH > Al_2O_3 ≫ $Al(OH)_3$, indicating that the support significantly impacts the activity of the catalyst in the ethanol-SCR process and AlOOH is the best precursor. Meanwhile, it is noteworthy that the N_2 production rate of 2 wt % Ag/Al_2O_3 derived from AlOOH and pretreated at 300 °C was worse than the counterpart derived from the Al_2O_3 precursor. Moreover, the peak in the curve for AlOOH-based catalysts was sharper than other curves, especially the Al_2O_3 series. For understanding the support effect and revealing the nature of the strongly peaked N_2 production rate curve, many characterization experiments were performed.

3.2. *In Situ* DRIFTS Studies. It is well-known that at the heart of HC-SCR of NOx over Ag/Al_2O_3 catalyst lies in the surface mechanism. With this in mind, *in situ* DRIFTS experiments were performed to take a closer look at support effects. HC-SCR of NOx usually starts with the partial oxidation of the reductant; thus, *in situ* DRIFTS spectra were collected over different Ag/Al_2O_3 samples in a flow of C_2H_5OH (1565 ppm) + O_2 (10%) over the temperature range 200−500 °C (the data are displayed in Figure S3). For convenience of comparison, Figure 2 shows the *in situ* DRIFT spectra at reaction temperature of 300 °C over Ag/Al_2O_3 catalysts derived from different precursors at steady state, all of which were calcined at the optimum temperature of 600 °C.

Exposure of different samples to the feed gas resulted in the appearance of six peaks (1668, 1633, 1565, 1470, 1410, and 1336 cm^{-1}) within the range of 2000−1200 cm^{-1}. According to earlier studies,[27,33−37] peaks at 1633 and 1410 cm^{-1} together with 1336 cm^{-1} were assigned to the asymmetric and symmetric stretching vibrations and C−H deformation vibration of adsorbed enolic species, respectively. Peaks at 1565 and 1470 cm^{-1} were due to acetate species adsorbed on the catalyst surface.[38,39] The partially oxidized species,

DOI: 10.1021/jp5114416
J. Phys. Chem. C 2015, 119, 3132−3142

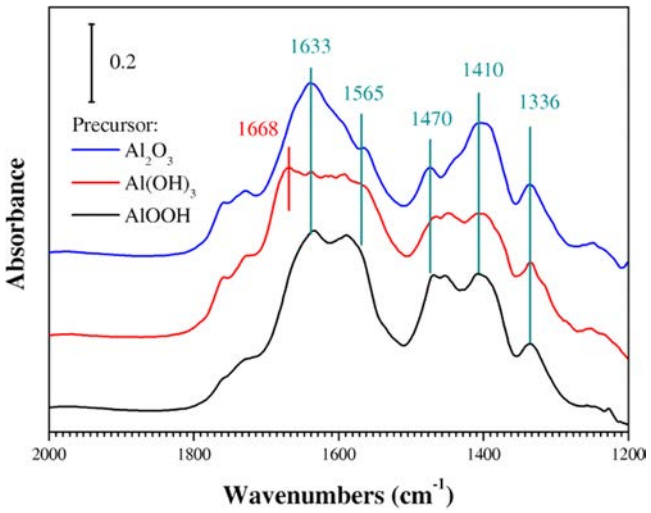

Figure 2. *In situ* DRIFTS spectra of adsorbed species on 2 wt % Ag/Al_2O_3 catalysts derived from different precursors and calcined at 600 °C at steady state in a flow of $C_2H_5OH + O_2$ at temperature of 300 °C.

especially the enolic species, were identified as important intermediates in the ethanol-SCR process because of their higher activity toward NO + O_2 than acetate, even though the latter was also formed during the partial oxidation of ethanol.[27,33−37] Comparing the different catalysts pretreated at 600 °C, it is clear that enolic species and acetate species were dominant on Al_2O_3, especially AlOOH-derived samples rather than $Al(OH)_3$-derived catalysts. As for the $Al(OH)_3$-based catalyst, the peak of 1668 cm^{-1} became dominant. We tentatively assign this peak to the C═O stretching vibration of acetone species. The peak close to the IR frequencies of acetone in the fundamental region is around 1700 cm^{-1}.[40]

To confirm the assignment, an acetone adsorption experiment was carried out, with the result shown in Figure 3A. As we can see, the peaks at 1668 and 1434 cm^{-1} appeared when the sample $Al(OH)_3$-600 was exposed to acetone (C_3H_6O) + O_2 at 300 °C. Thus, we can confirm that an acetone species is the main product of oxidation of ethanol on the $Al(OH)_3$-related sample. The conversion of ethanol into acetone also has been confirmed by other work,[41] during which iron oxide is the catalyst. A consecutive reaction may take place to form acetone: dehydrogenation of ethanol to acetaldehyde, aldol condensation of the acetaldehyde, and the reaction of the aldol with the lattice oxygen on the catalyst to form surface intermediate, followed by its dehydrogenation and decarboxylation.[42]

Subsequently, the reactivity of the adsorbed acetone species formed during the $C_2H_5OH + O_2$ reaction on $Al(OH)_3$-600 toward NO + O_2 was evaluated by the transient response of the DRIFTS method (Figure 3B). After the catalyst was exposed to $C_2H_5OH + O_2$ for 60 min, a strong peak (1668 cm^{-1}) due to the acetone species adsorbed on the surface was observed, along with the formation of enolic species (1336 and 1410 cm^{-1}; the peak of 1633 cm^{-1} was possibly masked by the strong peak at 1668 cm^{-1}). Switching the feed gas to NO + O_2 resulted in the appearance of peaks at 2240 cm^{-1}, which can be ascribed to −NCO species bound on the surface of the catalyst, while −CN species (around 2150 cm^{-1}) was barely observed in this study, which is consistent with other work.[20,28,43] The −NCO species is a vital intermediate for the SCR of NO_x by ethanol, usually formed by the consumption of enolic species and acetate species.[27,33−37] In this case, the appearance of

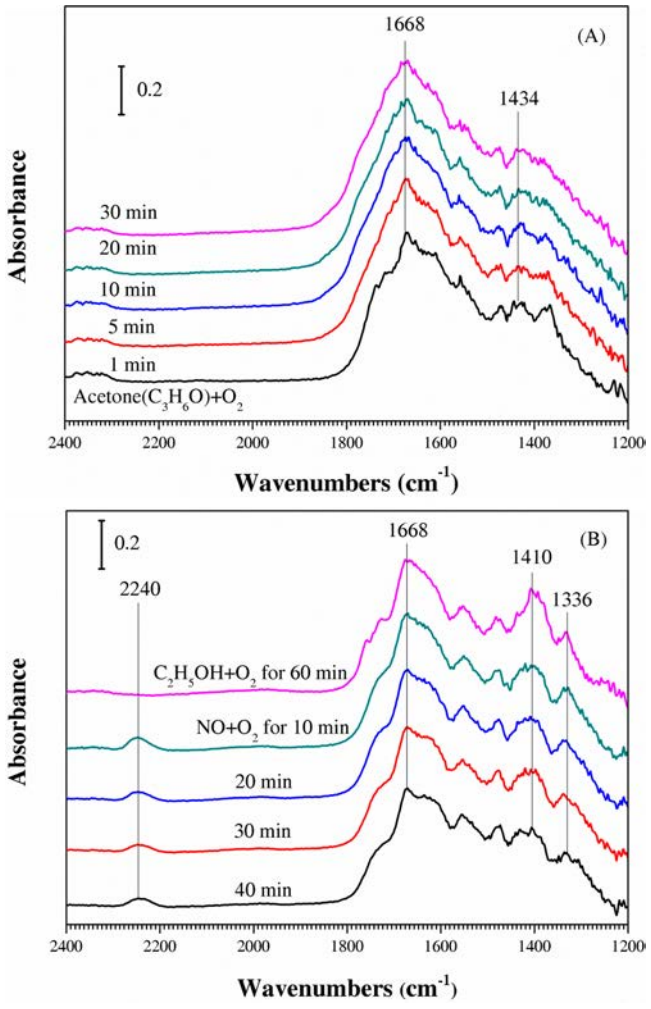

Figure 3. (A) Dynamic changes of *in situ* DRIFTS spectra of 2 wt % Ag/Al_2O_3 (derived from $Al(OH)_3$ at 600 °C) in flow of acetone + O_2 at 300 °C. (B) Dynamic changes of *in situ* DRIFTS spectra over 2 wt % Ag/Al_2O_3 (derived from $Al(OH)_3$ at 600 °C) as a function of time at 300 °C in N_2 purging followed by exposure to $C_2H_5OH + O_2$ and NO + O_2 in sequence.

−NCO species was also accompanied by the decrease in the intensity of enolic peaks (1410 cm^{-1}), while no remarkable decrease of acetone species was observed. Therefore, we can summarize that Ag/Al_2O_3 catalysts derived from $Al(OH)_3$ are selective to form acetone species rather than highly active enolic species during the partial oxidation of ethanol; the lower activity of acetone toward NO + O_2 to produce −NCO thus contributes to $Al(OH)_3$-600 having the lowest activity for NOx reduction. In order to clearly compare the reactivity of enolic species and −NCO among different catalysts, a trace amount of H_2 was added during transient response of the DRIFTS experiments. Over catalysts AlOOH-600 and Al_2O_3-600, the partial oxidation species (such as enolic species, with feature frequencies at 1633, 1410, and 1336 cm^{-1}) quickly disappeared, and −NCO species (2240 cm^{-1}) were formed instantaneously and then also disappeared, while very slow changes are observed over $Al(OH)_3$-600 catalyst as shown in Figure S4. It indicates that intermediates over catalysts AlOOH-600 and Al_2O_3-600 are more reactive than that over $Al(OH)_3$-600.

As described above, the surface mechanism is very important in the HC-SCR process. In the catalytic activity test section, we

DOI: 10.1021/jp5114416
J. Phys. Chem. C 2015, 119, 3132−3142

found a typical strongly peaked curve for N_2 production rate vs calcination temperature. To reveal the nature of the curve, *in situ* DRIFT spectra for the partial oxidation of ethanol over Ag/Al_2O_3 catalysts calcined at different temperatures were also compared. Taking catalysts derived from AlOOH as examples, C_2H_5OH + O_2 reactions carried out on 2 wt % Ag/Al_2O_3 catalysts (AlOOH-300, AlOOH-600, and AlOOH-900) are compared in Figure 4A. It can be seen clearly that the

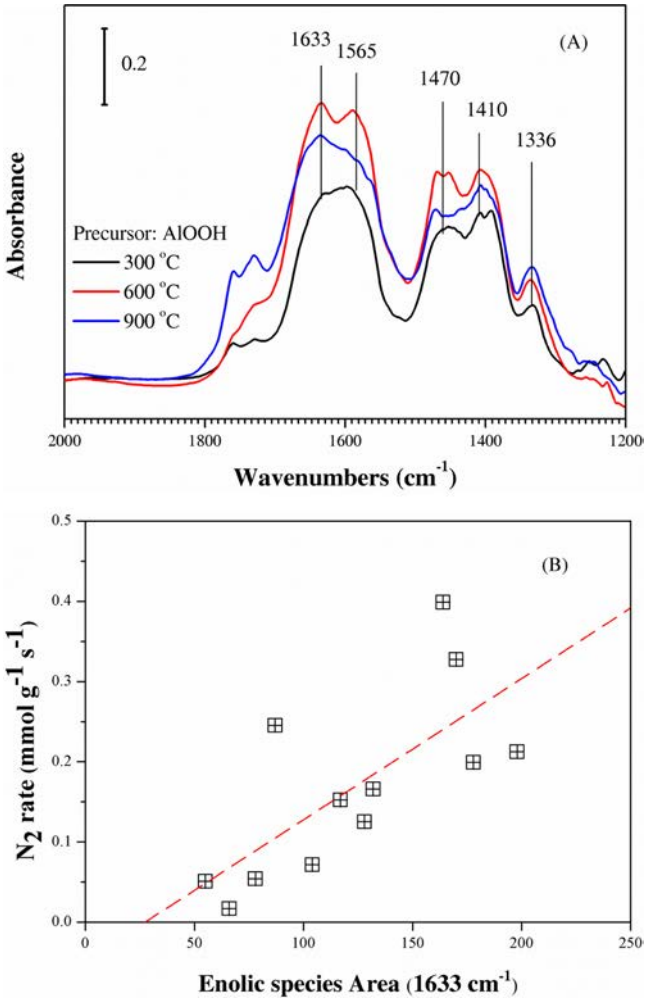

Figure 4. (A) *In situ* DRIFTS spectra of adsorbed species on 2 wt % Ag/Al_2O_3 catalysts derived from AlOOH (calcined at 300, 600, and 900 °C) at steady state in a flow of C_2H_5OH + O_2 at 300 °C. (B) Relationship between enolic species with N_2 production rate among different precursors.

intensities of peaks due to vital intermediate enolic species were strongly correlated with our former strongly peaked curve, varying in the order AlOOH-600 > AlOOH-900 > AlOOH-300. In order to qualitatively correlate N_2 production rate with partial oxidant of ethanol, enolic speices amounts formed under partial oxidation of ethanol at 300 °C over different catalysts were calculated by fitting on the basis of the deconvoluted curves after Kubelka−Munk conversion (take precursor AlOOH as an example, as shown in Figure S6). Figure 4B shows the trend between enolic species amount with N_2 production rate. It is clearly that enolic species amount is almost correlated with N_2 production rate linearly. Thus, a conclusion can be made that N_2 production is highly depended on vital surface intermediates like enolic species. However, the detailed Ag/Al_2O_3 catalyst structure as a function of calcination temperature and the related activity in the HC-SCR reaction is an open question.

3.3. Structural Properties. Generally, oxidized silver species present as isolated Ag^+ cations or/and oxidized silver clusters ($Ag_n^{\delta+}$) on the Al_2O_3 surface are crucial for the HC-SCR process.[44−47] Thus, the valence states of supported Ag for all samples were characterized by XPS, with the results shown in Table S1. The Ag $3d_{5/2}$ binding energy peaks for all samples appeared at around 368.5−369.1 eV, which is close to the range reported in previous studies.[44,48,49] Compared with the references of $AgNO_3$ and Ag_2O (the Ag $3d_{5/2}$ binding energies are 368.31 and 368.05 eV, respectively), we postulate that oxidized silver species are predominant on Ag/Al_2O_3 catalysts generally. To further reveal the constitution of silver species, UV−vis DRS experiments were performed, which are more reliable at learning the valence state of silver species. Taking the catalysts derived from three supports at 600 °C as examples, the UV−vis spectra and Gaussian deconvolutions on the basis of previous assignments[18,20] are presented in Figure S7. Generally, peaks appearing at 220 and 260 nm can be assigned to silver ions (Ag^+) and oxidized silver clusters ($Ag_n^{\delta+}$), respectively, while peaks centered at 290, 350, and 450 nm are due to metallic silver clusters (Ag_n^0).[20,22,45] It is clear that the absorbance peaks due to Ag^+ ions (220 nm) are predominant among all silver species for catalysts derived from precursor AlOOH and Al_2O_3. Silver metal species is predominant on surface of $Al(OH)_3$ derived samples. It is consistent with other work[22,23,26] that silver metal cluster accelerate unselective combustion of reductant. The formation of unreactive acetone speices on $Al(OH)_3$ derived catalyst may attribute to the predominant silver metal clusters. In contrast, silver ions should be considered as the active sites on Ag/Al_2O_3 catalysts. Nevertheless, the anchoring sites for silver ions on the Ag/Al_2O_3 surface may be quite different due to the support effect. Thus, the catalyst structural phases as influenced by alumina precursors and calcination temperature were compared.

The XRD patterns of uncalcined samples, compared with catalysts prepared at different temperatures, are shown in Figure S8. The peaks of the uncalcined precursor of AlOOH were identified as belonging to boehmite (PDF#01-088-2112) shown in Figure S8A, and after being calcined at 300 and 400 °C, both catalysts still maintained the boehmite (PDF #01-088-2112) structural phase. The physical structures of both catalysts such as surface area were also very similar as shown in Table 1. However, the catalytic performance of the sample pretreated at 400 °C was considerably higher than that calcined at 300 °C as shown in Figure 1. Further increasing the calcination temperature to 600 °C, the structural phase of the catalyst transformed into the γ-Al_2O_3 phase (PDF #00-010-0425), over which the highest N_2 production rate was achieved as shown in Figure 1. It is widely accepted that γ-Al_2O_3 is the activated form of alumina and thus commonly used as catalyst or support.[50] That would be part of the reason why the optimum pretreatment temperature was 600 °C in this study. However, raising the calcination temperature to 900 °C, the structural phase of catalyst transformed into the δ-Al_2O_3 phase (PDF #00-047-1770), over which the catalytic efficiency decreased significantly. Comparing the textual parameters of catalysts listed in Table 1, it can be seen that the surface areas were substantially reduced during the high temperature calcination at 900 °C. In the case of catalysts derived from the precursors

DOI: 10.1021/jp5114416
J. Phys. Chem. C 2015, 119, 3132−3142

Table 1. Textural Parameters of Ag/Al_2O_3 Catalysts with Different Silver Loadings Derived from N_2 Physisorption Results

sample	BET surf area (m^2/g)	pore vol (mL/g)	mean pore diam (nm)
AlOOH	276.6	0.41	5.96
Ag/Al_2O_3-300	214.3	0.41	7.59
Ag/Al_2O_3-400	238.7	0.48	7.99
Ag/Al_2O_3-600	213.1	0.51	9.54
Ag/Al_2O_3-900	141.9	0.48	13.61
$Al(OH)_3$			
Ag/Al_2O_3-300	260.6	0.20	3.02
Ag/Al_2O_3-400	261.9	0.23	3.44
Ag/Al_2O_3-600	168.1	0.26	6.11
Ag/Al_2O_3-900	87.6	0.26	12.02
Al_2O_3	185.8	0.49	10.52
Ag/Al_2O_3-300	200.2	0.47	9.41
Ag/Al_2O_3-400	193.5	0.48	9.86
Ag/Al_2O_3-600	197.9	0.52	10.48
Ag/Al_2O_3-900	145.5	0.46	12.55

$Al(OH)_3$ and Al_2O_3, we also found similar correlations between the catalysts' structure change and corresponding N_2 production rates. The common feature is that high temperature treatment (at 900 °C) is not beneficial to the catalytic performance. The δ-Al_2O_3 phase, probably due to its small surface area, has worse performance than the γ-Al_2O_3 phase in deNOx by ethanol. Thus, the discussion emphasis in the next section will focus on the temperature effects below 900 °C. In other words, we will focus on the issue of structure and activity relationship in the low temperature range (300−600 °C) of the rate curves.

Additionally, it is noteworthy that the catalysts derived from the Al_2O_3 precursor always maintain the γ-Al_2O_3 crystal phase throughout the pretreatment temperature range from 300 to 600 °C (as shown in Figure S8C). Meanwhile, the corresponding curve of N_2 production rate is relatively smooth. In order to determine the basic reason underlying the phenomenon, the Al coordination environments of all catalysts derived from different precursors and calcination temperatures were analyzed by ^{27}Al MAS NMR characterization as shown in Figure 5. The metal−support interactions were also interpreted.

It can be clearly seen in Figure 5 that two Al coordination structures were observed. The peak centered at 7.5 ppm can be assigned to Al^{3+} cations in octahedral coordination (thereafter, denoted as Al_{octa}), while the feature at 65 ppm can be attributed to tetrahedral coordination (thereafter, denoted as Al_{tetra}).[51−54] As for the uncalcined precursors AlOOH and $Al(OH)_3$, NMR

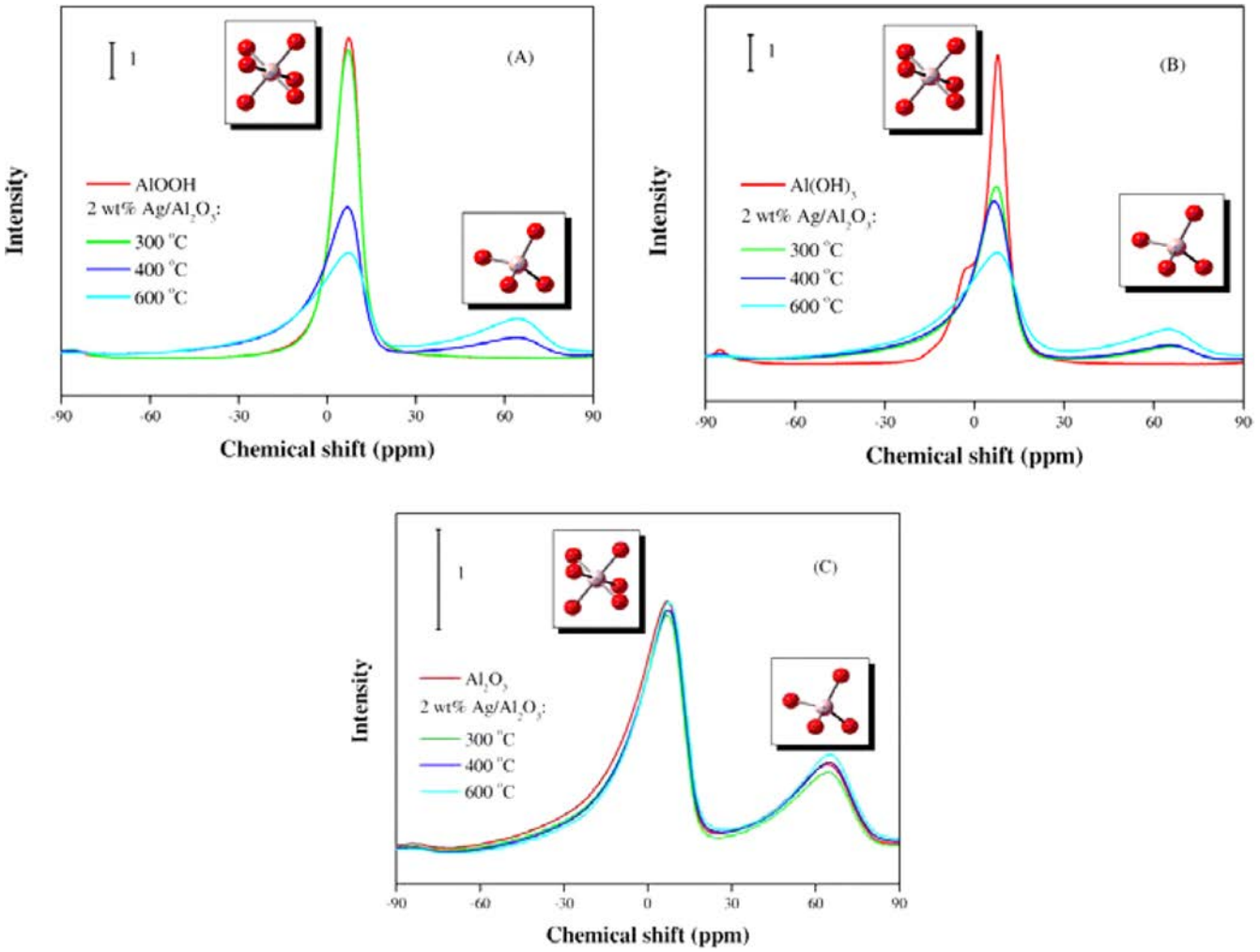

Figure 5. Solid-state ^{27}Al MAS NMR spectra of 2 wt % Ag/Al_2O_3 catalysts calcined at different temperatures (300, 400, and 600 °C) and derived from different alumina precursors: (A) AlOOH, (B) $Al(OH)_3$, and (C) Al_2O_3.

DOI: 10.1021/jp5114416
J. Phys. Chem. C 2015, 119, 3132−3142

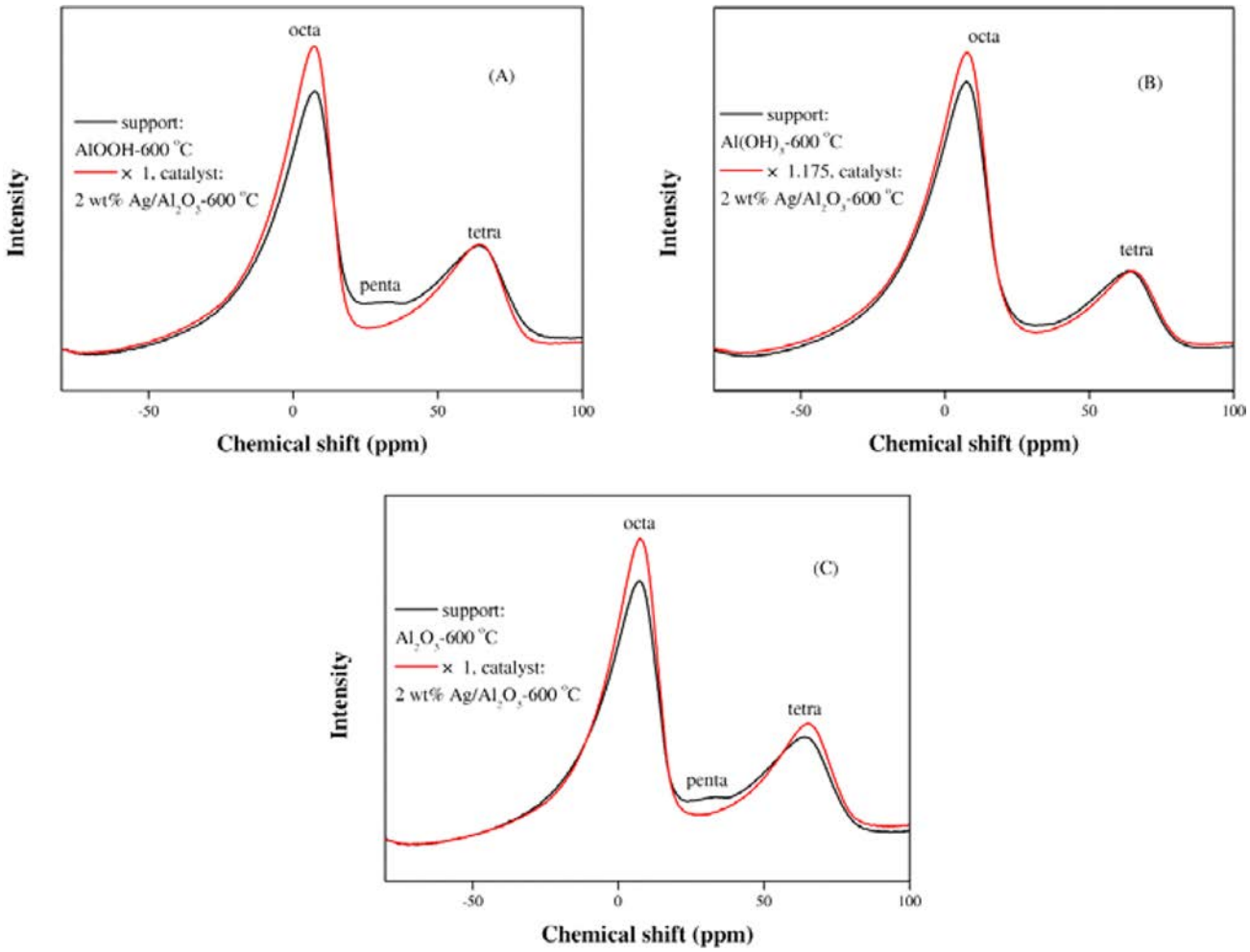

Figure 6. Solid-state ^{27}Al MAS NMR spectra of Ag/Al_2O_3 catalysts and corresponding supports calcined at 600 °C: (A) AlOOH, (B) $Al(OH)_3$, and (C) Al_2O_3.

results indicated that only Al_{octa} coordination can be found (as shown in Figure 5A,B). However, with the increase of calcination temperature from 300 to 600 °C, the intensity of the peak for Al_{octa} coordination gradually decreased, accompanied by the gradual increase of Al_{tetra} coordination.

The Al coordination structures and the related deNOx activity were interpreted next. For example, the Ag/Al_2O_3 catalyst derived from AlOOH at 300 °C is worse than the same material pretreated at 400 °C in terms of reduction of NO_x, as shown in Figure 1. It is worth keeping in mind that both samples present the same crystal phase and similar surface areas as discussed above. Nevertheless, if we check the detailed coordination structure of both catalysts, huge differences can be found. As shown in Figure 5A, the sample derived at 400 °C exhibited clear evidence of Al_{tetra} coordination; however, the sample prepared at 300 °C still maintained the Al_{octa} coordination structure, without any transformation observed. Further increasing the calcination temperature to 600 °C, the intensity of the peak corresponding to the Al_{tetra} structure continued to increase, at which point the best NO_x reduction performance was achieved. Moreover, another observation can also support the important role of Al_{tetra} played in HC-SCR process. As we described in the catalytic performance section, the strongly peaked curve of N_2 production rate belonging to Al_2O_3 is relatively smooth, for which the sample prepared at 300 °C was better than that derived from AlOOH at the same calcination temperature. The principal factor can also be attributed to the presence of the Al_{tetra} coordination. The Al_2O_3 precursor is different from AlOOH and $Al(OH)_3$ because Al_{tetra} is present in Al_2O_3 even at ambient temperature. But AlOOH cannot attain the Al_{tetra} structure until it is calcined at 400 °C. Moreover, the intensity of the peak corresponding to Al_{tetra} coordination in the Al_2O_3 precursor did not show obvious improvement when calcined from 300 to 600 °C. That could be the reason why its N_2 production rate curve is relatively smooth. Combining the NO_x reduction results as shown in Figure 1 with the ^{27}Al NMR characterization results, therefore, we assumed that Al_{tetra} coordination plays a crucial role in ethanol-SCR.

3.4. Structure−Activity Relationship. As described above, the coordination structures of framework Al in supports are crucial in the reduction of NO_x. But it is noteworthy that silver species such as oxidized silver are commonly considered as the active species. In our recent work,[20] we also proposed that activated HC intermediates like enolic species prefer to selectively adsorb on or close to silver sites. Burch et al.[19] also suggest that the interface between active silver and alumina contributed to the adsorption of reactive species like isocyanate. Thus, clarifying the detailed interaction between the silver species and support framework Al requires understanding the role that the Al skeleton plays in the HC-SCR process and to further learn the structure−activity relationship.

DOI: 10.1021/jp5114416
J. Phys. Chem. C 2015, 119, 3132−3142

In order to elucidate the interaction between the active Ag species and framework Al, solid-state ^{27}Al MAS NMR spectra of the bare supports and silver compound catalysts calcined at the same temperature of 600 °C were compared as shown in Figure 6. The new peak centered at 35 ppm can be assigned to an Al^{3+} cation in pentahedral coordination in the bare support (thereafter, denoted as Al_{penta}).[51−54] As for precursors AlOOH and Al_2O_3, after silver loading, the Al_{penta} coordination structure disappeared, and meanwhile, the Al_{oct} coordination increased as shown in Figure 6A,C. This indicates that the Al_{penta} site might be the silver ion anchoring spot to form an Ag−O−Al_{octa} entity. However, the support $Al(OH)_3$ was deficient in Al_{penta} sites as shown in Figure 6B. That may lead to enhanced formation of silver metal species as mentioned before in Figure S7B, which eventually caused inactive intermediate acetone species to be formed on the surface and, consequently, lowered the corresponding reduction efficiency of NOx. The peak of Al_{tetra} remained almost unchanged after silver loading for the precursors AlOOH and Al_2O_3. However, we cannot arbitrarily exclude the possibility that silver species can bond with Al_{tetra} sites to form Ag−O−Al_{tetra} entities. For instance, silver ions may exchange with a proton from hydroxyl groups that bond with Al_{tetra} on alumina surface. In that case, the NMR peak of Al_{tetra} was barely influenced by its coordination environment and Ag−O−Al_{tetra} can form.

Herein, we conclude that there are two kinds of stable Al coordination on Ag/Al_2O_3 catalysts, as the solid-state ^{27}Al MAS NMR spectra shown in Figure 6. Thus, the predominant silver ions presumably have two possible anchoring sites. With the aid of DFT calculation, we constructed the two detailed Ag−O−Al_{tetra} and Ag−O−Al_{octa} entities as shown in Figure S9. Silver ion anchored on Al_{III} site[31,32,50] on Al_2O_3(110) surface via O bridge can form Ag−O−Al_{tetra} entity, which had been confirmed by our previous study.[21] A silver ion attached to Al_{penta} site[31,32] on Al_2O_3(100) surface via O bridge can produce the Ag−O−Al_{octa} entity. The formation energy of Ag−O−Al_{tetra} (−1.56 eV) is much higher than that of Ag−O−Al_{octa} (−3.41 eV), indicating the Ag−O−Al_{octa} is more stable than Ag−O−Al_{tetra} and should be the more typical of Ag−O−Al entity. Other studies[53,54] also support Al_{octa} as the common site environment for anchoring active species such as for the noble metal Pt, which is consistent with our results in Figure 6. Herein, we can conclude that the Al_{penta} site is the energetically favorable site to anchor silver ions, which then support the silver ions to form Ag−O−Al_{octa} entities. As for Ag/Al_2O_3, some other reports[24,25] suggest that the Al_{tetra} silver phase is the active structure. On the basis of catalytic performance and NMR characterization, we also propose that the Al_{tetra} structure is crucial in NOx reduction indeed. To further reveal the function of the Al_{tetra}, the relationship between the amount of Al_{tetra} structure and N_2 production rate was correlated.

The N_2 production rates as a function of the amount of Al tetracoordination are plotted in Figure 7. Note that the percentages of Al coordination were calculated and shown in Table 2 and Table S2. It is clear that with increasing amount of Al_{tetra} the N_2 production rate increased monotonically for all catalysts regardless of the precursor. Thus, we can conclude that Al_{tetra} plays an important role in N_2 production. Silver species presumably anchored on Al_{tetra} sites are the active sites. In order to confirm the true active site between Ag−O−Al_{tetra} and Ag−O−Al_{octa} entities, the vital intermediates −NCO species adsorbed on both entities were compared by DFT calculations. The configuration of −NCO species on Ag−O−Al entities are displayed in Figure 8. The adsorption energies for −NCO adsorbed on Ag−O−Al_{tetra} and Ag−O−Al_{octa} entities are −3.84 and −3.49 eV, respectively, indicating that Ag−O−Al_{tetra} entity promote the adsorption of −NCO rather than Ag−O−Al_{octa} entity. After adsorption, small deformation of −NCO was observed. For instance, the N−C and C−O bond lengths in free isocynate acid are 1.227 and 1.185 Å, respectively. The corresponding N−C bond in −NCO adsorbed on Ag−O−Al_{tetra} and Ag−O−Al_{octa} entities are 1.236 and 1.215 Å, respectively, while the C−O bond increase to 1.196 and 1.203 Å correspondingly. In summary, Ag−O−Al_{tetra} has better ability to activate −NCO species obviously than Ag−O−Al_{octa} entity since the elongation of both N−C and C−O bonds. Combined with the experimental and theoretical results, the amount of Al_{tetra} is directly related with the production rate of N_2, which confirms the important role of Al coordination environment in reducing NOx. However, it is well-known that the bare support Al_2O_3 with Al_{tetra} cannot perform good catalytic activity during HC-SCR process without active silver phases[21] especially at low temperatures. The interactions between predominant silver ions and support Al site are identified as crucial in this study. Burch et al.[19] and Yu et al.[20] also found that the interface between silver species and the alumina support might be the active site. On the basis of DFT calculation, Ag−O−Al entities were constructed and Ag−O−Al_{tetra} rather than Ag−O−Al_{octa} can activate vital intermediates −NCO species significantly. Thus, we can conclude that Ag−O−Al_{tetra} rather than Ag−O−Al_{octa} entities should be considered as active sites during the HC-SCR process.

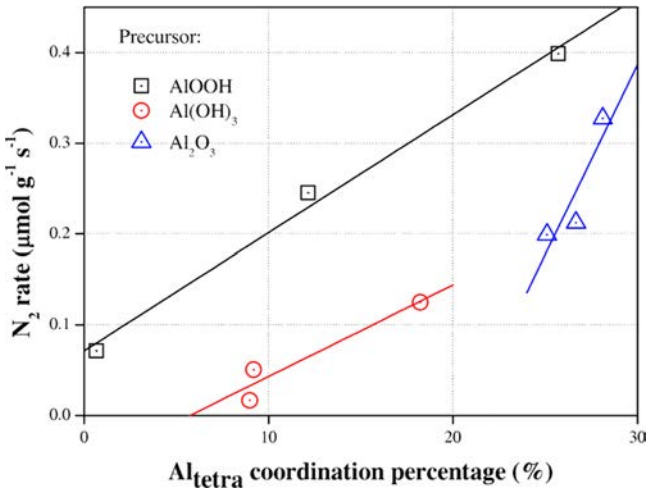

Figure 7. Relationship between N_2 production rate during ethanol-SCR and relative amount of Al_{tetra} coordination in Ag/Al_2O_3 catalysts.

Table 2. Percentages of Al_{tetra} and Al_{octa} Structures in 2 wt % Ag/Al_2O_3 Catalysts and Precursors

sample	Al_{tetra} (%)	Al_{octa} (%)	sample	Al_{tetra} (%)	Al_{octa} (%)
AlOOH	0	100	Al_2O_3	25.2	74.8
AlOOH-300	0.6	99.4	Al_2O_3-300	25.1	74.9
AlOOH-400	12.1	87.9	Al_2O_3-400	26.6	73.4
AlOOH-600	25.7	74.3	Al_2O_3-600	28.1	71.9
$Al(OH)_3$	0	100			
$Al(OH)_3$-300	8.9	91.1			
$Al(OH)_3$-400	9.2	90.8			
$Al(OH)_3$-600	18.2	81.8			

DOI: 10.1021/jp5114416
J. Phys. Chem. C 2015, 119, 3132−3142

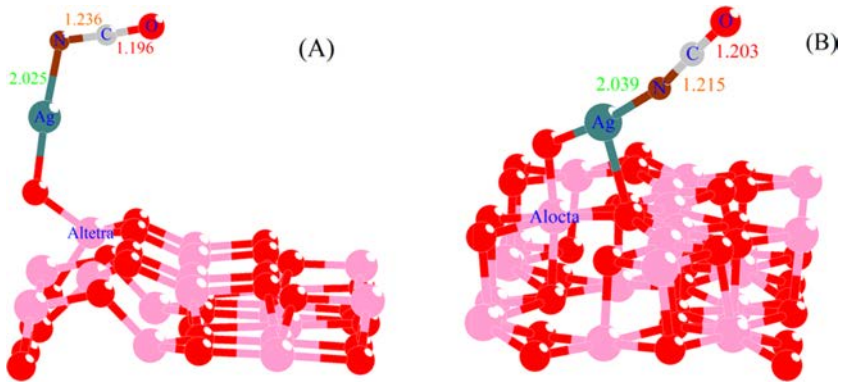

Figure 8. Structure of the −NCO adsorbed on Ag/Al_2O_3 catalyst: (A) on $Ag-O-Al_{tetra}$ entity; (B) on $Ag-O-Al_{octa}$ entity.

4. CONCLUSIONS

For the ethanol-SCR process, it is found that the general order of NO_x reduction efficiency as affected by precursors can be described as $AlOOH > Al_2O_3 \gg Al(OH)_3$. The relatively low performance of silver catalysts derived from $Al(OH)_3$ may be attributable to the formation of inactive surface acetone species during the partial oxidation of ethanol. Typical strongly peaked curves of N_2 production rate vs calcination temperature are found for all kinds of supports in this study, and the optimum calcination temperature is 600 °C. Tracking the structure change of catalysts, we found that Ag−O−Al entities may be composed of $Ag-O-Al_{tetra}$ and $Ag-O-Al_{oct}$ structures. NMR and DFT calculation suggest that Al_{oct} rather than Al_{tetra} is the energetically preferable coordination site to bond silver ions. The lack of Al_{penta} sites on the precursor $Al(OH)_3$ to form the $Ag-O-Al_{oct}$ entity causes enhanced formation of silver metal species, which likely eventually lowers the reduction of NOx. A strongly positive correlation between the amount of Al_{tetra} coordination and N_2 production rate confirms the crucial role of Al_{tetra} in NOx reduction by ethanol. DFT calculations indicate that $Ag-O-Al_{tetra}$ entities adsorb and activate vital intermediate −NCO species more profoundly than over $Ag-O-Al_{octa}$ entities and should be considered as active sites.

■ ASSOCIATED CONTENT

Ⓢ Supporting Information

Activity of Ag/Al_2O_3 for ethanol-SCR, *in situ* DRIFTS, UV−vis DRS spectra, deconvolution of UV−vis DRS spectra, XPS, XRD, NMR, and DFT calculation. This material is available free of charge via the Internet at http://pubs.acs.org.

■ AUTHOR INFORMATION

Corresponding Author

*E-mail: honghe@rcees.ac.cn (H.H.).

Author Contributions

The manuscript was written through contributions of all authors. All authors have given approval to the final version of the manuscript. H.D. and Y.Y. contributed equally.

Notes

The authors declare no competing financial interest.

■ ACKNOWLEDGMENTS

The work was supported by the National Natural Science Foundation of China (21373261 and 21177142) and the National High Technology Research and Development Program of China (863 Program, 2013AA065301).

■ REFERENCES

(1) Burch, R.; Breen, J. P.; Meunier, F. C. A Review of the Selective Reduction of NOx with Hydrocarobns under Lean-Burn Conditions with Non-Zeolite Oxide and Plantinum Group Metal Catalysts. *Appl. Catal., B* **2002**, *39*, 283−303.

(2) Shimizu, K. I.; Satsuma, A. Selective Catalytic Reduction of NO over Supported Silver Catalyst-Practical and Mechanistic Aspects. *Phys. Chem. Chem. Phys.* **2006**, *8*, 2677−2695.

(3) Liu, Z. M.; Woo, S. I. Recent Advances in Catalytic DeNOx Science and Technology. *Catal. Rev.* **2006**, *48*, 43−89.

(4) He, H.; Zhang, X. L.; Wu, Q.; Zhang, C. B.; Yu, Y. B. Review of Ag/Al_2O_3-Reductant System in the Selective Catalytic Reduction of NOx. *Catal. Surv. Asia* **2008**, *12*, 38−55.

(5) Granger, P.; Parvulescu, V. I. Catalytic NOx Abatement Systems for Mobile Sources: From Three-Way to Lean Burn after-Treatment Technologies. *Chem. Rev.* **2011**, *111*, 3155−3207.

(6) Iwamoto, M.; Yahiro, H.; Shundo, S.; Yu-u, Y.; Mizuno, N. Selective Reduction of NO by Lower Hydrocarbons in the Presence of O_2 and SO_2 over Copper Ion-Exchanged Zeolites. *Shokubai (Catalyst)* **1990**, *32*, 430−433.

(7) Held, W.; König, A.; Richter, T.; Pupper, L. Catalytic NOx Reduction in Net Oxidizing Exhaust Gas. *SAE [Tech. Pap.]* **1990**, 900496.

(8) Pârvulescu, V. I.; Grange, P.; Delmon, B. Catalytic Removal of NO. *Catal. Today* **1998**, *46*, 233−316.

(9) Habib, H. A.; Basner, R.; Brandenburg, R.; Armbruster, U.; Martin, A. Selective Catalytic Reduction of Ship Diesel Engine Exhaust Gas with C_3H_6 over Cu/Y Zeolite. *ACS Catal.* **2014**, *4*, 2479−2491.

(10) Burch, R.; Millingtopn, P. J.; Walker, A. P. Mechanism of the Selective Reduction of Nitrogen Monoxide on Platinum-Based Catalysts in the Presence of Excess Oxygen. *Appl. Catal., B* **1994**, *4*, 65−94.

(11) Satsuma, A.; Shimizu, K. I. In Situ FT/IR Study of Selective Catalytic Reduction of NO over Alumina-Based Catalysts. *Prog. Energy Combust.* **2003**, *29*, 71−84.

(12) Meunier, F. C.; Ross, J. R. H. Effect of Ex Situ Treatments with SO_2 on the Activity of a Low Loading Silver-Alumina Catalyst for the Selective Reduction of NO and NO_2 by Propene. *Appl. Catal., B* **2000**, *24*, 23−32.

(13) Bethke, K. A.; Kung, H. H. Supported Ag Catalysts for the Lean Reduction of NO with C_3H_6. *J. Catal.* **1997**, *172*, 93−102.

(14) He, H.; Zhang, R. D.; Yu, Y. B. Selective Catalytic Reduction of NO in the Presence of Excess Oxygen I. SCR of NO with C_3H_6 over Ag/Al_2O_3. *Chin. J. Catal.* **2003**, *24*, 788−794.

(15) Stere, C. E.; Adress, W.; Burch, R.; Chansai, S.; Goguet, A.; Graham, W. G.; Rosa, F. D.; Palma, V.; Hardacre, C. Ambient Temperature Hydrocarbon Selective Catalytic Reduction of NOx Using Atmospheric Pressure Nonthermal Plasma Activation of a Ag/Al_2O_3 Catalyst. *ACS Catal.* **2014**, *4*, 666−673.

DOI: 10.1021/jp5114416
J. Phys. Chem. C 2015, 119, 3132−3142

(16) Haneda, M.; Kintaichi, Y.; Inaba, M.; Hamada, H. Infrared Study of Catalytic Reduction of Nitrogen Monoxide by Propene over Ag/TiO_2-ZrO_2. *Catal. Today* **1998**, *42*, 127−135.
(17) Satokawa, S.; Shibata, J.; Shimizu, K. I.; Satsuma, A.; Hattori, T. Promotion Effect of H_2 on the Low Temperature Activity of the Selective Reduction of NO by Light Hydrocarbons over Ag/Al_2O_3. *Appl. Catal., B* **2003**, *42*, 179−186.
(18) She, X.; Stephanopoulos, M. F. The Role of Ag-O-Al Species in Silver-Alumina Catalysts for the Selective Catalytic Reduction of NOx with Methane. *J. Catal.* **2006**, *237*, 79−93.
(19) Chansai, S.; Burch, R.; Hardacre, C.; Breen, J.; Meunier, F. The Use of Short Time-on-Stream In Situ Spectroscopic Transient Kinetic Isotope Techniques to Investigate the Mechanism of Hydrocarbon Selective Catalytic Reduction (HC-SCR) of NOx at Low Temperatures. *J. Catal.* **2011**, *281*, 98−105.
(20) Yan, Y.; Yu, Y. B.; He, H.; Zhao, J. J. Intimate Contact of Enolic Species with Silver Sites Benefits the SCR of NOx by Ethanol over Ag/Al_2O_3. *J. Catal.* **2012**, *293*, 13−26.
(21) Deng, H.; Yu, Y. B.; Liu, F. D.; Ma, J. Z.; Zhang, Y.; He, H. The Nature of Ag Species in Ag/γ-Al_2O_3: A Combined Experimental and Theoretical Study. *ACS Catal.* **2014**, *4*, 2776−2784.
(22) Yoon, D. Y.; Park, J. H.; Kang, H. C.; Kim, P. S.; Nam, I. S.; Yeo, G. K.; Kil, J. K.; Cha, M. S. DeNOx Performance of Ag/Al_2O_3 Catalyst by n-Dodecane: Effect of Calcination Temperature. *Appl. Catal., B* **2011**, *101*, 275−282.
(23) Zhang, R. D.; Kaliaguine, S. Lean Reduction of NO by C_3H_6 over Ag/Alumina Derived from Al_2O_3, AlOOH and $Al(OH)_3$. *Appl. Catal., B* **2008**, *78*, 275−287.
(24) Bion, N.; Saussey, J.; Haneda, M.; Daturi, M. Study by In Situ FTIR Spectroscopy of the SCR of NOx by Ethanol on Ag/Al_2O_3-Evidence of the Role of Isocyanate Species. *J. Catal.* **2003**, *217*, 47−58.
(25) Iglesias-Juez, A.; Hungria, A. B.; Martinez-Arias, A.; Fuerte, A.; Fernandez-Garcia, M. Nature and Catalytic Role of Active Silver Species in the Lean NOx Reduction with C_3H_6 in the Presence of Water. *J. Catal.* **2003**, *217*, 310−323.
(26) He, H.; Zhang, C. B.; Yu, Y. B. A Comparative Study of Ag/Al_2O_3 and Cu/Al_2O_3 Catalysts for the Selective Catalytic Reduction of NO by C_3H_6. *Catal. Today* **2004**, *90*, 191−197.
(27) He, H.; Yu, Y. B. Selective Catalytic Reduction of NOx over Ag/Al_2O_3 Catalyst: From Reaction Mechanism to Diesel Engine Test. *Catal. Today* **2005**, *100*, 37−47.
(28) Yu, Y. B.; Zhao, J. J.; Yan, Y.; Han, X.; He, H. A Cyclic Reaction Pathway Triggered by Ammonia for the Selective Catalytic Reduction of NOx by Ethanol over Ag/Al_2O_3. *Appl. Catal., B* **2013**, *136−137*, 103−111.
(29) Costa, C. N.; Efstathiou, A. M. Low-Temperature H_2-SCR of NO on a Novel Pt/MgO-CeO_2 Catalyst. *Appl. Catal., B* **2007**, *72*, 240−252.
(30) Valanidou, L.; Theologides, C.; Zorpas, A. A.; Savva, P. G.; Costa, C. N. A Novel Highly Selective and Stable Ag/MgO-CeO_2-Al_2O_3 Catalyst for the Low-Temperature Ethanol-SCR of NO. *Appl. Catal., B* **2011**, *107*, 164−176.
(31) Digne, M.; Sautet, P.; Raybaud, P.; Euzen, P.; Toulhoat, H. Priority Communication Hydroxyl Groups on γ-Alumina Surfaces: A DFT Study. *J. Catal.* **2002**, *211*, 1−5.
(32) Digne, M.; Sautet, P.; Raybaud, P.; Euzen, P.; Toulhoat, H. Use of DFT to Achieve a Rational Understanting of Acid-Basic Properties of γ-Alumina Surfaces. *J. Catal.* **2004**, *226*, 54−68.
(33) Yu, Y. B.; He, H.; Feng, Q. C. Novel Enolic Surface Species Fromed during Parital Oxidation of CH_3CHO, C_2H_5OH, and C_3H_6 on Ag/Al_2O_3: An In Situ DRIFTS Study. *J. Phys. Chem. B* **2003**, *107*, 13090−13092.
(34) Yu, Y. B.; Gao, H. W.; He, H. FTIR, TPD and DFT Studies of Intermediates on Ag/Al_2O_3 during the Selective Catalytic Reduction of NO by C_2H_5OH. *Catal. Today* **2004**, *93−95*, 805−809.
(35) Wu, Q.; He, H.; Yu, Y. B. In Situ DRIFTS Study of the Selective Reduction of NOx with Alcohols over Ag/Al_2O_3 Catalyst: Role of Surface Enolic Species. *Appl. Catal., B* **2005**, *61*, 107−113.
(36) Gao, H. W.; He, H.; Yu, Y. B. Density Functianl Theory (DFT) and DRIFTS Investigations of the Formation and Adsorption of Enolic Species on the Ag/Al_2O_3 Surface. *J. Phys. Chem. B* **2005**, *109*, 13291−13295.
(37) Yu, Y. B.; Song, X. P.; He, H. Remarkable Influence of Reductant Structure on the Activity of Alumina-Supported Silver Catalyst for the Selective Catalytic Reduction of NOx. *J. Catal.* **2010**, *271*, 343−350.
(38) Meunier, F. C.; Breen, J. P.; Zuzaniuk, V.; Olsson, M.; Ross, J. R. H. Mechanistic Aspects of the Selective Reduciton of NO by Propene over Alumina and Silver-Alumina Catalysts. *J. Catal.* **1999**, *187*, 493−505.
(39) Shimizu, K. I.; Shibata, J.; Yosida, H.; Satsuma, A.; Hattori, T. Silver-Alumina Catalysts for Selective Reduciton of NO by Higher Hydrocarbons: Structure of Active Sites and Reaction Mechanism. *Appl. Catal., B* **2001**, *30*, 151−162.
(40) Chen, Y. J.; Morisawa, Y.; Futami, Y.; Czarnecki, M. A.; Wang, H. S.; Ozaki, Y. Combined IR/NIR and Density Functional Theory Calculations Analysis of the Solvent Effects on Frequencies and Intensities of the Fundamental and Overtones of the C═O Stretching Vibrations of Acetone and 2-Hexanone. *J. Phys. Chem. A* **2014**, *118*, 2576−2583.
(41) Hino, M.; Arata, K. Conversion of Ethanol into Acetone Catalysed by Iron Oxide Treated with Tellurate Ion. *J. Chem. Soc., Chem. Commun.* **1988**, *1168*, 393−395.
(42) Nishiguchi, T.; Matsumoto, T.; Kanai, H.; Utani, K.; Matsumura, Y.; Shen, W. J.; Imamura, S. Catalytic Steam Reforming of Ethanol to Produce Hydrogen and Acetone. *Appl. Catal., A* **2005**, *279*, 273−277.
(43) Zhang, X. L.; Yu, Y. B.; He, H. Effect of Hydrogen on Reaction Intermediates in the Selective Catalytic Reduction of NOx by C_3H_6. *Appl. Catal., B* **2007**, *76*, 241−247.
(44) He, H.; Li, Y.; Zhang, X. L.; Yu, Y. B.; Zhang, C. B. Precipitable Silver Compound Catalysts for the Selective Catalytic Reduction of NOx by Ethanol. *Appl. Catal., A* **2010**, *375*, 258−264.
(45) Breen, J. P.; Burch, R.; Hardacre, C.; Hill, C. J. Structural Investigation of the Promotional Effect of Hydrogen during the Selective Catalytic Reduction of NOx with Hydrocarbons over Ag/Al_2O_3 Catalysts. *J. Phys. Chem. B* **2005**, *109*, 4805−4807.
(46) Shimizu, K. I.; Tsuzuki, M.; Kato, K.; Yokota, S.; Okumura, K. Satsuma, A. Reductive Activation of O_2 with H_2-Reduced Silver Clusters as a Key Step in the H_2-Promoted Selective Catalytic Reduction of NO with C_3H_8 over Ag/Al_2O_3. *J. Phys. Chem. C* **2007**, *111*, 950−959.
(47) Korhonen, S. T.; Beale, A. M.; Newton, M. A.; Weckhuysen, B. M. New Insights into the Active Surface Species of Silver Alumina Catalysts in the Selective Catalytic Reduction of NO. *J. Phys. Chem. C* **2011**, *115*, 885−896.
(48) Tjeng, L. H.; Meinders, M. B. J.; Ghijsen, J. E. J.; Sawatzky, G. A. Electronic Structure of Ag_2O. *Phys. Rev. B* **1990**, *41*, 3190−3199.
(49) Kannisto, H.; Ingelsten, H. I.; Skoglundh, M. Ag-Al_2O_3 Catalysts for Lean NOx Reduction-Influence of Preparation Method and Reductant. *J. Mol. Catal. A: Chem.* **2009**, *302*, 86−96.
(50) Wischert, R.; Laurent, P.; Coperet, C.; Delbecq, F.; Sautet, P. γ-Alumina: The Essential and Unexpected Role of Water for the Structure, Stability, and Reactivity of "Defect" Sites. *J. Am. Chem. Soc.* **2012**, *134*, 14430−14449.
(51) Kwak, J. H.; Hu, J. Z.; Kim, D. H.; Szanyi, J. S.; Peden, C. H. F. Penta-Coordinated Al^{3+} Ions as Preferential Nucleation Sites for BaO on γ-Al_2O_3: An Ultra-High-Magnetic Field ^{27}Al MAS NMR Study. *J. Catal.* **2007**, *251*, 189−194.
(52) Kwak, J. H.; Hu, J. Z.; Lukaski, A.; Kim, D. H.; Szanyi, J. S.; Peden, C. H. F. Role of Pentacoordinated Al^{3+} Ions in the High Temperature Phase Transformation of γ-Alumina. *J. Phys. Chem. C* **2008**, *112*, 9486−9492.
(53) Kwak, J. H.; Mei, D. H.; Yi, C. W.; Kim, D. H.; Peden, C. H. F.; Allar, L. F.; Szanyi, J. Understanding the Nature of Surface Nitrates in BaO/γ-Al_2O_3 NOx Storage Materials: A Combined Experimental and Theoretical Study. *J. Catal.* **2009**, *261*, 17−22.

DOI: 10.1021/jp5114416
J. Phys. Chem. C 2015, 119, 3132−3142

(54) Kwak, J. H.; Hu, J. Z.; Mei, D. H.; Yi, C. W.; Kim, D. H.; Peden, C. H. F.; Allar, L. F.; Szanyi, J. Coordinatively Unsaturated Al^{3+} Centers as Binding Sites for Active Catalyst Phases of Platinum on γ-Al_2O_3. *Science* **2009**, *325*, 1670−1673.

DOI: 10.1021/jp5114416
J. Phys. Chem. C 2015, 119, 3132−3142